

Manipulating non-Hermitian skin effect via electric fields

Yi Peng,^{1,2,3,*} Jianwen Jie,^{1,2,3,*} Dapeng Yu,^{1,2,3} and Yucheng Wang^{1,2,3,†}

¹Shenzhen Institute for Quantum Science and Engineering,
Southern University of Science and Technology, Shenzhen 518055, China

²International Quantum Academy, Shenzhen 518048, China

³Guangdong Provincial Key Laboratory of Quantum Science and Engineering,
Southern University of Science and Technology, Shenzhen 518055, China

In non-Hermitian systems, the phenomenon that the bulk-band eigenstates are accumulated at the boundaries of the systems under open boundary conditions is called the non-Hermitian skin effect (NHSE), which is one of the most iconic and important features of a non-Hermitian system. In this work, we investigate the fate of NHSE in the presence of electric fields by analytically calculating the dynamical evolution of an initial bulk state and numerically computing the spectral winding number, the distributions of eigenstates, as well as the dynamical evolutions. We show the abundant suppression effects of dc and ac fields on the NHSE based on the physical mechanisms that the interplay between the Stark localization or dynamic localization and the NHSE. In addition, the finite size analysis of the non-Hermitian system with a pure dc field also shows the phenomenon of size-dependent NHSE. The results will help to deepen the understanding of NHSE and its manipulation.

Introduction.— Hermiticity of Hamiltonian has been regarded as a fundamental requirement in standard quantum mechanics, and it ensures the conservation of probability and energy-values being real in an isolated system, yet many systems, such as the nonequilibrium and open systems with gain and loss, can be effectively described by the non-Hermitian Hamiltonian. Especially in recent years, non-Hermitian physics has attracted widespread attention in both theory [1–16] and experiment [17–23]. Various unique features of non-Hermitian systems without any Hermitian counterparts have been revealed, such as exceptional points and rings [24–33], enriched topological classifications [5, 6, 34–39], and non-Hermitian skin effect (NHSE) [7, 8, 10, 19, 21, 40–43]. In NHSE, macroscopically many bulk-band eigenstates are localized at the system boundary with open boundary conditions (OBC), which drastically reshapes the bulk-boundary correspondence principle and motivates the finding of generalized Brillouin zone [7–9].

Now we focus on how to manipulate the NHSE, one of the most iconic properties of the non-Hermitian systems. If introducing a new term in the non-Hermitian Hamiltonian with NHSE, and it can drive the skin modes into the bulk, i.e., suppressing the NHSE. Then the non-Hermitian effect may be eliminated, and the system may have the conservation of probability and all the eigenvalues may be real, even though the non-Hermitian term remains. Thus, manipulating NHSE is helpful for deepening our understanding of non-Hermitian quantum mechanics and the differences between Hermitian and non-Hermitian physics. Moreover, if grasping how to control the NHSE, one can obtain or remove it in accordance with requirements. Therefore, manipulating NHSE also has practical significance. Two recent work [44, 45] have studied the interplay between the magnetic fields and NHSE in two dimensional non-Hermitian systems, and found that a small magnetic field was sufficient to sup-

press NHSE. A natural question is that whether the electric field as another basic regulation mechanism can also manipulate the NHSE, and if it can also suppress NHSE, whether it can bring richer and more interesting physics?

Aiming to answer the above questions, in this work we investigate the interplay between the electric fields and NHSE in one dimensional (1D) non-Hermitian systems, and obviously, the NHSE of 1D systems can not be manipulated by the magnetic fields. We firstly analytically study the dynamical behavior of a particle initially localized at the bulk, and whether it will move toward the boundary can reveal the existence or non-existence of the NHSE. Then we consider three cases: the presence of the pure dc field, pure ac field, and the mixed field of dc and ac electric fields and study their effects on the NHSE analytically and numerically.

Model and results.— We consider a 1D non-Hermitian system with non-reciprocal hopping under the influence of electric field, and the Hamiltonian is written as

$$\hat{H} = \sum_n (J_L |n\rangle\langle n+1| + J_R |n+1\rangle\langle n|) + E(t)a \sum_n n |n\rangle\langle n|, \quad (1)$$

where $|n\rangle$ is the Wannier state localized on the lattice site n , $J_L(J_R)$ represents the leftward (rightward) hopping amplitude, a is the lattice constant, being set as 1 throughout this work, and $E(t) = e\xi(t)$, with e and $\xi(t)$ being the charge on the particle and external electric field respectively.

We can analytically confirm the existence or disappearance of NHSE by investigating the motion of a particle, this is because the particle initially localized on the bulk should move toward the boundary if there exists the NHSE. We firstly substitute an arbitrary time-dependent quantum state $|\psi(t)\rangle = \sum_m C_m(t)|m\rangle$ into the Schrödinger equation $i\partial_t|\psi(t)\rangle = \hat{H}(t)|\psi(t)\rangle$ and obtain the eigen-equation for the time-dependent ampli-

tudes $C_m(t) = \langle m|\psi(t)\rangle$,

$$i\partial_t C_m(t) = J_L C_{m+1}(t) + J_R C_{m-1}(t) + mE(t)C_m(t). \quad (2)$$

Here we set $\hbar = 1$. By solving the Eq. (2), for arbitrary

time dependence of $E(t)$, we can obtain the exact solutions of the quantum dynamics,

$$C_m(t) = \sum_r (-1)^{m-r} C_r(0) e^{-i\eta(t)r} J_{m-r} \left(2\sqrt{J_L J_R [\mathcal{U}^2(t) + \mathcal{V}^2(t)]} \right) \left[\frac{J_R i\mathcal{V}(t) - \mathcal{U}(t)}{J_L i\mathcal{V}(t) + \mathcal{U}(t)} \right]^{\frac{m-r}{2}}. \quad (3)$$

Here $J_{m-r}(x)$ is the $(m-r)$ th order Bessel function of the first kind, $\mathcal{U}(t) = \int_0^t \cos[\eta(t) - \eta(t')] dt'$ and $\mathcal{V}(t) = \int_0^t \sin[\eta(t) - \eta(t')] dt'$ with

$$\eta(t) = \int_0^t E(t') dt'. \quad (4)$$

This solution is valid for arbitrary initial bulk state $|\psi(0)\rangle$ and for any time-dependent electric field $E(t)$, and the details for the calculation are put in the Supplementary Materials [46]. To simplify the expression and without loss of generality, we consider the specific initial states that only occupy in a single Wannier lattice site n_0 , namely $|\psi(0)\rangle = |n_0\rangle$, and then the probability amplitude at any site m after evolution time t , $\rho_m(t) = |C_m(t)|^2$, takes [46]

$$\rho_m(t) = \mathcal{J}_{m-n_0}^2 \left(2\sqrt{J_L J_R [u^2(t) + v^2(t)]} \right) \left(\frac{J_R}{J_L} \right)^{m-n_0}, \quad (5)$$

with

$$u(t) = \int_0^t dt' \cos \eta(t'), \quad v(t) = \int_0^t dt' \sin \eta(t'). \quad (6)$$

In the absence of electric field, i.e., $E(t) = 0$, from Eq. (4) and Eq. (6), we have $u(t) = t$ and $v(t) = 0$, yielding $\rho_m(t) = \mathcal{J}_{m-n_0}^2 (2t\sqrt{J_L J_R}) (J_R/J_L)^{m-n_0}$, where $2t\sqrt{J_L J_R}$ is linearly increasing to infinity and thus $\mathcal{J}_{m-n_0}(2t\sqrt{J_L J_R})$ approaches to vanish [47] [see Fig. 1(a)], such that $\rho_m/\rho_{m-1} \approx J_R/J_L$ when $t \rightarrow \infty$. Therefore, the system has right (left) boundary skin mode when $J_R/J_L > 1$ ($J_R/J_L < 1$), which is consistent with previous results [7, 8, 10]. The following sections will discuss three cases: i) the pure dc field case with $E(t) = E_0$ being time-independent, ii) the pure ac field case with $E(t) = E_1 \cos(\omega t)$, and iii) the mixed field case with $E(t) = E_0 + E_1 \cos(\omega t)$.

The pure dc electric field case.— We firstly discuss the fate of NHSE in the presence of a pure dc electric field, $E(t) = E_0$. From Eq. (4) and Eq. (6), we have $u(t) = \frac{\sin E_0 t}{E_0}$ and $v(t) = \frac{1 - \cos E_0 t}{E_0}$, and then, Eq. (5) gives the probability amplitude:

$$\rho_m(t) = \mathcal{J}_{m-n_0}^2 \left(\frac{4\sqrt{J_L J_R}}{E_0} \sin \frac{E_0 t}{2} \right) \left(\frac{J_R}{J_L} \right)^{m-n_0}. \quad (7)$$

It can be seen that $\sin \frac{E_0 t}{2} = 0$ at the time points $t^* = 2\pi N/E_0$ with $N = 0, 1, 2, \dots$. By using the property of the Bessel function [47] $\mathcal{J}_{m-n_0}(0) = \delta_{m-n_0,0}$ [see Fig. 1(a)] and $(J_R/J_L)^{m-n_0} = 1$ when $m = n_0$, we have that the probability amplitude $\rho_{m=n_0}(t^*)$ will oscillate back to 1 whatever the initial site n_0 is, which actually, corresponds to the Stark localization [48], and thus, the particle initially localized at the bulk does not move toward the boundary. Therefore, the effect of the interplay between the Stark localization and NHSE is that a small dc electric field is sufficient to suppress the NHSE.

The analytical results can be further confirmed by numerically calculating the winding number (WN), eigenstates' distributions and dynamical evolution. Under periodic boundary conditions (PBC), the system with NHSE will have a persistent current. Thus, the NHSE corresponds to a delocalized phase under PBC. Whether the NHSE exists [6, 41, 43] and the localized properties [12–14] of a eigenstate can be characterized by the WN of the spectrum around the corresponding eigenvalue. To define the WN, we need introduce the twist boundary condition here, i.e., $\hat{H}(\Phi) = \hat{H} + J_L e^{i\Phi}|L\rangle\langle 1| + J_R e^{-i\Phi}|1\rangle\langle L|$, where L is the system size and Φ is the introduced phase factor, and then define the WN

$$w = \frac{1}{2\pi i} \int_0^{2\pi} \partial_\Phi \ln \det [\hat{H}(\Phi) - \mathcal{E}_c] d\Phi. \quad (8)$$

$w = 0$ ($w = 1$) for localized (delocalized) state or the non-existence (existence) of NHSE with eigenvalue around \mathcal{E}_c , which is set to the algebra average of the spectrum in the following calculation. For convenience, we set $J_L = J - \gamma/2$ and $J_R = J + \gamma/2$ with $\gamma > 0$ and $J = 1$ as the unit of energy. Fig. 1 (b) shows the localized-delocalized transition with different sizes L obtained by calculating the WN, and when E_0 increased cross the line with fixed L from left to right, the WN change from 0 to 1. With increasing L , the transition point E_0^c tends to zero for any γ , which is consistent with the analytical result.

The analytical expression of $\rho_m(t)$ can also tell us the finite size effect. Here, we consider $J_R > J_L$, which makes the oscillation of the bulk initial state that would favor the right-band side of the initial position n_0 , and the

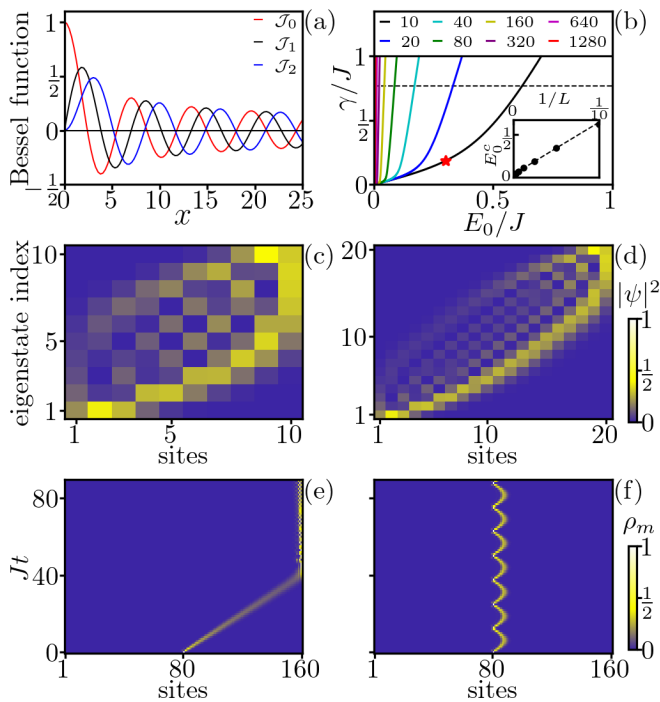


Figure 1: (a) The distributions of the zero-th, first and second order Bessel function. We can see two used characteristics in the text: the amplitudes of oscillation decrease with increasing x and when $x \rightarrow \infty$, $G_m(x) \rightarrow 0$ for any m ; $G_0(0) = 1$ and $G_m(0) = 0$ when $m \neq 0$, so we have $G_m(0) = \delta_{m,0}$. (b) Localization-delocalization transition characterized by winding number for finite lattices. The inset shows transition dc field strength E_0^c versus $1/L$, given $\gamma = 0.77$ marked as dashed line in its parent figure. The distributions of eigenstates with (c) system size $L = 10$ and (d) $L = 20$, and other parameters are $\gamma = 0.185$ and $E_0 = 0.3$ as marked by red star in (b). Numerical integration of Schrödinger equation of electron started from the lattice center under (e) the weak dc field with $E_0 = 0.005$ and (f) the strong dc field with $E_0 = 0.5$, and other parameters are $L = 160$, $\gamma = 0.769$.

range of the oscillation is approximate to $4J_R/|E_0|x_*$ [46], where x_* only depends on J_L and J_R . Thus, $\rho_m(t) \approx 0$ when $m - n_0 > 4J_R/|E_0|x_*$ or $m - n_0 < 0$. If the distance between the right-side boundary and n_0 is larger than $4J_R/|E_0|x_*$, the particle will return back to n_0 after a period of time, but if the distance is less than $4J_R/|E_0|x_*$, the particle will arrive at the boundary and then stay there ever since, which suggests the number of the skin modes is about $4J_R/|E_0|x_*$, being not dependent on the lattice size L . Therefore, for fixed size L , there exist a critical electric field strength E_0^c that satisfies $4J_R/|E_0^c|x_* = L$ make all states be skin modes, which gives the relation $E_0^c \propto 1/L$, as shown in the inset of Fig 1 (b). Fig 1 (c) shows the distributions of the eigenstates of the system at a transition point, and we see that the number of the skin modes equals to $L/2$, this is because the \mathcal{E}_c in Eq. (8) we chose is near the middle

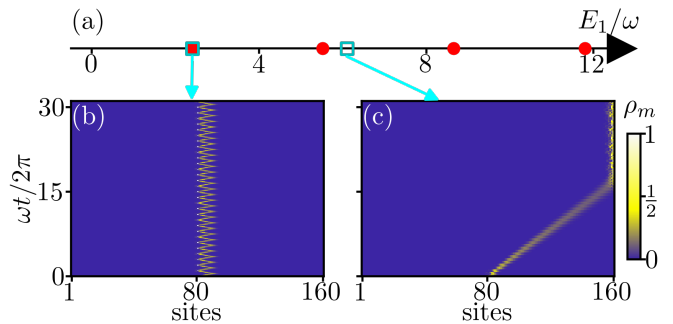


Figure 2: (a) Red round dots are zeros of zeroth order of the Bessel function $\mathcal{J}_0(E_1/\omega)$, which correspond to the condition of the emergence of the dynamic localization under ac field driving. Dynamical evolution of a particle initially localized at the lattice center with (b) $E_1/\omega = 2.405$, which is the first zero point of $\mathcal{J}_0(E_1/\omega)$ and (c) $E_1/\omega = 6.1$. Here we set $J = 1$, $\gamma = 0.73$, and $\omega = 0.46$.

of the energy spectrum here. With increasing the system size, as we discussed above, the number of the skin modes remains unchanged, as shown in Fig 1 (d). Thus, with fixing J_L , J_R and E_0 , the number of the skin modes can be of the same order of magnitude as the total eigenstate number for the system with small size and display the NHSE, and when the size is large enough, the ratio of the number of skin modes to the total eigenstate number will be insignificant and the NHSE will disappear, which is consistent with the analytical results. The phenomenon of the size-dependent NHSE, i.e., NHSE only appearing at small system sizes, as far as we know, has not been revealed by previous work. From the above discussions, we can increase the number of skin modes by decreasing the electric field strength E_0 , and thus, we can control the appearance or disappearance of NHSE for a finite size system, as shown in Fig 1 (e) and (f). It can be seen that when $E_0 = 0.005$, the system with $L = 160$ shows the NHSE, and the particle moves toward to the boundary, but when $E_0 = 0.5$, most of the particles initially localized in the bulk will oscillate around the initial position.

The pure ac electric field case.— We then consider the monochromatic cosine shape ac electric field $E = E_1 \cos(\omega t)$. It is a typical Floquet driving system, with period $T = 2\pi/\omega$. From Eq. (4) and Eq. (6), we have $u(t) = \int_0^t dt' \cos(\frac{E_1}{\omega} \sin \omega t')$ and $v(t) = \int_0^t dt' \sin(\frac{E_1}{\omega} \sin \omega t')$, and then, Eq. (5) gives the probability amplitude in the limit of long evolution time $t \gg T$ [46],

$$\rho_m(t \gg T) \approx \mathcal{J}_{m-n_0}^2 \left(2t\sqrt{J_L J_R} \mathcal{J}_0\left(\frac{E_1}{\omega}\right) \right) \left(\frac{J_R}{J_L}\right)^{m-n_0} \quad (9)$$

When $\mathcal{J}_0(E_1/\omega) \neq 0$, $2t\sqrt{J_L J_R} \mathcal{J}_0(E_1/\omega)$ will increase linearly to infinity and thus $\mathcal{J}_{m-n_0}(2t\sqrt{J_L J_R} \mathcal{J}_0(E_1/\omega))$ will tend to zero, which is completely similar to the case

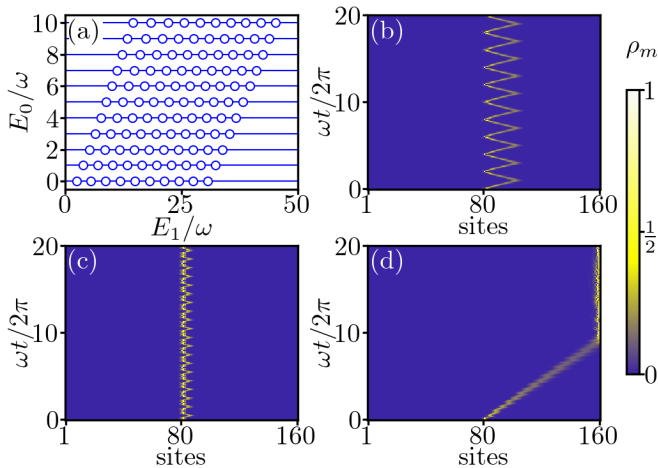


Figure 3: (a) The schematic phase diagram about the existence or non-existence of NHSE under the mixed electric field driving consist of dc and ac components. Blue lines correspond to the integer E_0/ω , where the particle can move towards to by the photon absorption or emission. The hollow circles on the blue lines correspond to E_1/ω being the zeroes of $\mathcal{J}_{E_0/\omega}$, where the dynamic localization induced by the ac electric field occur. In the white region between the blue lines, the NHSE disappears because of the Stark localization. The dynamical evolutions of the electron initialized on the lattice center under simultaneous driving of dc and ac electric field with (b) $E_0/\omega = 0.5$ and $E_1/\omega = 1.3$, (c) $E_0/\omega = 1$ and $E_1/\omega = 3.832$ corresponding to the first zero of \mathcal{J}_1 , and (d) $E_0/\omega = 1$ and $E_1/\omega = 5.7$. Here we fix $J = 1$, $\gamma = 0.73$ and $\omega = 0.46$.

without electric field discussed above. In this condition, the NHSE will not be affected by the ac electric field. For the special ac field strength E_1 and its frequency ω that make $\mathcal{J}_0(E_1/\omega) = 0$, due to the property of the Bessel function $\mathcal{J}_{m-n_0}(0) = \delta_{m-n_0,0}$, the particle initially localized the bulk will not move toward the boundary, and thus, the NHSE will be suppressed. Red round dots in Fig 2(a) are zeroes of zeroth order of the Bessel function \mathcal{J}_0 , and it can be seen that the particle move around the initial position when when the ratio E_1/ω is chosen as one of the zeroes of \mathcal{J}_0 , as shown in Fig 2(a). This localization phenomenon is called dynamic localization [49–52], which is distinct from Anderson localization induced by random disorder potential. For most cases, $\mathcal{J}_0(E_1/\omega) \neq 0$, the particle will hop to the boundary eventually as demonstrated in Fig. 2(c). To sum up, when only ac electric field exists, the NHSE is not affected except for these special parameters of E_1 and ω that make the dynamic localization happen, which will suppress the NHSE.

The dc+ac electric field case.— We finally consider the effect of the combination of ac and dc electric fields, i.e., $E(t) = E_0 + E_1 \cos(\omega t)$, in manipulating the NHSE. By using Eq. (4) and Eq. (6), we can calculate $u(t)$ and $v(t)$, whose expressions look fair complicated (see Supplementary Materials [46]), and find that when E_0/ω

is not an integer, all the terms in the expressions of u and v are bounded oscillatory functions of time, meaning that the particle will oscillate around the initial position in the bulk. Therefore, the electric field with both dc and ac parts will break the NHSE if E_0/ω are not integers. When E_0/ω is equal to an integer, the expression of the probability amplitude in the limit of long evolution time [46] can be simplified to

$$\rho_m(t \gg T) \approx \mathcal{J}_{m-n_0}^2 \left(2t \sqrt{J_L J_R} \mathcal{J}_{\frac{E_0}{\omega}} \left(\frac{E_1}{\omega} \right) \right) \left(\frac{J_R}{J_L} \right)^{m-n_0}, \quad (10)$$

From the above expression, if E_0/ω is an integer, the discussions that similar to the case of the ac electric field can be done, i.e., the disappearance or existence of NHSE depends on whether E_1/ω is one of the zeroes of the Bessel function $\mathcal{J}_{E_0/\omega}$ or not. In the presence of the pure dc field E_0 , as discussions above, there exists the Stark localization, suppressing the NHSE. Then adding the ac field $E_1 \cos(\omega t)$, and when E_0/ω is an integer, the particle can break through the localization barrier and move through the chain accompanied by the photon absorption or emission. Thus, NHSE can exist under the conditions of integer E_0/ω except the situation of E_1/ω being the zero of $\mathcal{J}_{E_0/\omega}$, which will induce the dynamic localization, as discussions above. The effects of the mixed electric field of ac and dc fields on the NHSE are summarized in the Fig. 3(a). The white region between the blue lines and the hollow circles on the blue lines correspond to the non-integer E_0/ω and the zeroes of $\mathcal{J}_{E_0/\omega}$ respectively, which will induce the Stark localization and dynamic localization and lead to the disappearance of NHSE, as shown in Fig. 3(b) and (c). The blue lines correspond to the integer E_0/ω , which can break the bulk localization by photon assisted movement, and the particle initially localized in the bulk will move towards to the boundary, as shown in Fig. 3(d).

Summary.— We have investigated the control effect of electric fields on the NHSE analytically and numerically. For the pure dc field case, in the thermodynamic limit, a weak Stark localization induced by the dc field is sufficient to win the competition between the Stark localization and the NHSE, so a non-zero dc field can suppress the NHSE. When the system size is finite, the existence or non-existence of NHSE depends on leftward hopping amplitude J_L , rightward hopping amplitude J_R and the dc field strength E_0 , so one can manipulate the NHSE through multiple methods. For the pure ac field case, only the special situation with field strength E_1 and frequency ω that satisfy $\mathcal{J}_0(E_1/\omega) = 0$ can suppress the NHSE, whose physical mechanism is the dynamic localization suppressing the movement toward the boundary. For the mixed field case, if E_0/ω is not an integer, the NHSE will be suppressed by the Stark localization induced by the dc field. For the integer E_0/ω case, NHSE will exist, because the particle can move to-

ward the boundary by the photon absorption or emission except for the special case with E_1/ω being one of the zeroes of $\mathcal{J}_{E_0/\omega}$, which will induce the dynamic localization. The control effects of electric fields on the NHSE are abundant, moreover, electric fields can be easily added to a system. Thus, the manipulated methods can be widely used in experiments.

We thank L. Li and H. Jiang for valuable discussions. This work was supported by the National Natural Science Foundation of China (Grants No. U1801661, No.12104205), the Key-Area Research and Development Program of Guangdong Province (Grant No. 2018B030326001), Guangdong Provincial Key Laboratory (Grant No.2019B121203002).

* These authors contribute equally to this work.

† Corresponding author: wangyc3@sustech.edu.cn

- [1] Y. Ashida, Z. Gong, and M. Ueda, Non-Hermitian physics, *Advances in Physics* **69**, 249 (2020).
- [2] C. M. Bender and S. Boettcher, Real spectra in non-Hermitian Hamiltonians having PT-symmetry, *Phys. Rev. Lett.* **80**, 5243 (1998); C. M. Bender, D. C. Brody, and H. F. Jones, Complex extension of quantum mechanics, *Phys. Rev. Lett.* **89**, 270401 (2002).
- [3] N. Hatano and D. R. Nelson, Vortex pinning and non-Hermitian quantum mechanics, *Phys. Rev. B* **56**, 8651 (1997); N. Hatano and D. R. Nelson, Non-Hermitian delocalization and eigenfunctions, *Phys. Rev. B* **58**, 8384 (1998).
- [4] T. E. Lee, Anomalous edge state in a non-Hermitian lattice, *Phys. Rev. Lett.* **116**, 133903 (2016).
- [5] H. Shen, B. Zhen, and L. Fu, Topological band theory for non-Hermitian Hamiltonians, *Phys. Rev. Lett.* **120**, 146402 (2018).
- [6] Z. Gong, Y. Ashida, K. Kawabata, K. Takasan, S. Higashikawa, and M. Ueda, Topological phases of non-Hermitian systems, *Phys. Rev. X* **8**, 031079 (2018).
- [7] S. Yao and Z. Wang, Edge states and Topological invariants of non-Hermitian systems, *Phys. Rev. Lett.* **121**, 086803 (2018); S. Yao, F. Song, and Z. Wang, Non-Hermitian Chern bands, *Phys. Rev. Lett.* **121**, 136802 (2018).
- [8] F. K. Kunst, E. Edvardsson, J. C. Budich, and E. J. Bergholtz, Biorthogonal bulk-boundary correspondence in non-Hermitian systems, *Phys. Rev. Lett.* **121**, 026808 (2018).
- [9] Z. Yang, K. Zhang, C. Fang, and J. Hu, Non-Hermitian bulk-boundary correspondence and auxiliary generalized Brillouin zone theory, *Phys. Rev. Lett.* **125**, 226402 (2020).
- [10] C. H. Lee and R. Thomale, Anatomy of skin modes and topology in non-Hermitian systems, *Phys. Rev. B* **99**, 201103 (2019).
- [11] K. Kawabata, K. Shiozaki, M. Ueda, and M. Sato, Symmetry and topology in non-Hermitian physics, *Phys. Rev. X* **9**, 041015 (2019).
- [12] S. Longhi, Topological Phase Transition in non-Hermitian Quasicrystals, *Phys. Rev. Lett.* **122**, 237601 (2019); S. Longhi, Phase transitions in a non-Hermitian Aubry-Andre-Harper model, *Phys. Rev. B* **103**, 054203 (2021).
- [13] H. Jiang, L.-J. Lang, C. Yang, S.-L. Zhu, and S. Chen, Interplay of non-Hermitian skin effects and Anderson localization in non-reciprocal quasiperiodic lattices, *Phys. Rev. B* **100**, 054301 (2019).
- [14] Y. Liu, X. Jiang, J. Cao, and S. Chen, Non-Hermitian mobility edges in one-dimensional quasicrystals with parity-time symmetry, *Phys. Rev. B* **101**, 174205 (2020); Y. Liu, Y. Wang, Z. Zheng, and S. Chen, Exact non-Hermitian mobility edges in one-dimensional quasicrystal lattice with exponentially decaying hopping and its dual lattice, *Phys. Rev. B* **103**, 134208 (2021).
- [15] L. Zhou, Floquet engineering of topological localization transitions and mobility edges in one-dimensional non-Hermitian quasicrystals, *Phys. Rev. Research*, **3**, 033184 (2021).
- [16] E. J. Bergholtz, J. C. Budich, and F. K. Kunst, Exceptional topology of non-Hermitian systems, *Rev. Mod. Phys.* **93**, 015005 (2021).
- [17] H. Schomerus, Topologically protected midgap states in complex photonic lattices, *Opt. Lett.* **38**, 1912 (2013).
- [18] J. Li, A. K. Harter, J. Liu, L. de Melo, Y. N. Joglekar, and L. Luo, Observation of parity-time symmetry breaking transitions in a dissipative Floquet system of ultracold atoms, *Nat. Commun.* **10**, 855 (2019).
- [19] L. Xiao, T. Deng, K. Wang, G. Zhu, Z. Wang, W. Yi, and P. Xue, Non-Hermitian bulk-boundary correspondence in quantum dynamics, *Nat. Phys.* **16**, 761 (2020).
- [20] S. Weidemann, M. Kremer, T. Helbig, T. Hofmann, A. Stegmaier, M. Greiter, R. Thomale, and A. Szameit, Topological funneling of light, *Science* **368**, 311 (2020).
- [21] T. Helbig, T. Hofmann, S. Imhof, M. Abdelghany, T. Kiessling, L. Molenkamp, C. Lee, A. Szameit, M. Greiter, and R. Thomale, Generalized bulk-boundary correspondence in non-Hermitian topoelectrical circuits, *Nat. Phys.* **16**, 747 (2020).
- [22] X.-X. Zhang and M. Franz, Non-Hermitian exceptional Landau quantization in electric circuits, *Phys. Rev. Lett.* **124**, 046401 (2020).
- [23] W. Zhang, X. Ouyang, X. Huang, X. Wang, H. Zhang, Y. Yu, X. Chang, Y. Liu, D.-L. Deng, and L.-M. Duan, Observation of non-Hermitian topology with nonunitary dynamics of solid-state spins, *Phys. Rev. Lett.* **127**, 090501 (2021).
- [24] C. Dembowski, H.-D. Gräf, H. L. Harney, A. Heine, W. D. Heiss, H. Rehfeld, and A. Richter, Experimental observation of the topological structure of exceptional points, *Phys. Rev. Lett.* **86**, 787 (2001); C. Dembowski, B. Dietz, H.-D. Gräf, H. L. Harney, A. Heine, W. D. Heiss, and A. Richter, Encircling an exceptional point, *Phys. Rev. E* **69**, 056216 (2004).
- [25] J. Wiersig, Enhancing the sensitivity of frequency and energy splitting detection by using exceptional points: application to microcavity sensors for single-particle detection, *Phys. Rev. Lett.* **112**, 203901 (2014).
- [26] W. Hu, H. Wang, P. P. Shum, Y. D. Chong, Exceptional points in a non-Hermitian topological pump, *Phys. Rev. B* **95**, 184306 (2017).
- [27] W. Chen, Ş. K. Özdemir, G. Zhao, J. Wiersig, and L. Yang, Exceptional points enhance sensing in an optical microcavity, *Nature (London)* **548**, 192 (2017).
- [28] H. Hodaei, A. U. Hassan, S. Wittek, H. Garcia-Gracia, R.

- El-Ganainy, D. N. Christodoulides, and M. Khajavikhan, Enhanced sensitivity at higher-order exceptional points, *Nature (London)* **548**, 187 (2017).
- [29] M. Zhang, W. Sweeney, C. W. Hsu, L. Yang, A. D. Stone, and L. Jiang, Quantum noise theory of exceptional point amplifying sensors, *Phys. Rev. Lett.* **123**, 180501 (2019).
- [30] M.-A. Miri and A. Alù, Exceptional points in optics and photonics, *Science* **363**, eaar7709 (2019).
- [31] Y. Xu, S.-T. Wang, and L.-M. Duan, Weyl exceptional rings in a three-dimensional dissipative cold atomic Gas, *Phys. Rev. Lett.* **118**, 045701 (2017).
- [32] A. Cerjan, S. Huang, M. Wang, K. P. Chen, Y. Chong, and M. C. Rechtsman, Experimental realization of a Weyl exceptional ring, *Nat. Photonics* **13**, 623 (2019).
- [33] C. H. Lee, L. Li, and J. Gong, Hybrid higher-order skin-topological modes in nonreciprocal systems, *Phys. Rev. Lett.* **123**, 016805 (2019).
- [34] K. Kawabata, S. Higashikawa, Z. Gong, Y. Ashida, and M. Ueda, Topological unification of time-reversal and particle-hole symmetries in non-Hermitian physics, *Nat. Commun.* **10**, 297 (2019).
- [35] U. Magnea, Random matrices beyond the Cartan classification, *Journal of Physics A: Mathematical and Theoretical* **41**, 045203 (2008).
- [36] C. C. Wojcik, X.-Q. Sun, T. Bzdušek, and S. Fan, Homotopy characterization of non-Hermitian Hamiltonians, *Phys. Rev. B* **101**, 205417 (2020).
- [37] Z. Li and R. S. K. Mong, Homotopical classification of non-Hermitian band structures, *Phys. Rev. B* **103**, 155129 (2021).
- [38] H. Hu and E. Zhao, Knots and non-Hermitian Bloch bands, *Phys. Rev. Lett.* **126**, 010401 (2021).
- [39] C.-H. Liu and S. Chen, Topological classification of defects in non-Hermitian systems, *Phys. Rev. B* **100**, 144106 (2019); C.-H. Liu, H. Jiang, and S. Chen, Topological classification of non-Hermitian systems with reflection symmetry, *Phys. Rev. B* **99**, 125103 (2019).
- [40] V. M. M. Alvarez, J. E. B. Vargas, and L. E. F. F. Torres, Non-hermitian robust edge states in one dimension: Anomalous localization and eigenspace condensation at exceptional points, *Phys. Rev. B* **97**, 121401 (2018).
- [41] K. Zhang, Z. Yang, and C. Fang, Correspondence between winding numbers and skin modes in non-Hermitian systems, *Phys. Rev. Lett.* **125**, 126402 (2020); K. Zhang, Z. Yang, and C. Fang, Universal non-Hermitian skin effect in two and higher dimensions, arXiv:2102.05059.
- [42] Y. Yi and Z. Yang, Non-Hermitian skin modes induced by on-site dissipations and chiral tunneling effect, *Phys. Rev. Lett.* **125**, 186802 (2020).
- [43] N. Okuma, K. Kawabata, K. Shiozaki, and M. Sato, Topological origin of non-Hermitian skin effects, *Phys. Rev. Lett.* **124**, 086801 (2020).
- [44] M. Lu, X.-X. Zhang, and M. Franz, Magnetic suppression of non-Hermitian skin effects, *Phys. Rev. Lett.* **127**, 256402 (2021).
- [45] K. Shao, H. Geng, W. Chen, and D. Y. Xing, Interplay between non-Hermitian skin effect and magnetic field: skin modes suppression, Onsager quantization and MT phase transition, arXiv:2111.04412.
- [46] See Supplemental Material for details on (I) deriving the analytical solutions of quantum dynamics; (II) discussing the analytical results; (III) the finite size effect in the pure dc field case. The Supplemental Materials includes the references [47, 53, 54].
- [47] G. N. Watson, *A Treatise on the Theory of Bessel Functions*, Cambridge Mathematical Library (Cambridge University Press, 1995).
- [48] G. H. Wannier, Dynamics of band electrons in electric and magnetic fields, *Rev. Mod. Phys.* **34**, 645 (1962).
- [49] D. H. Dunlap and V. M. Kenkre, Dynamic localization of a charged particle moving under the influence of an electric field, *Phys. Rev. B* **34**, 3625 (1986); D. H. Dunlap and V. M. Kenkre, Dynamic localization of a particle in an electric field viewed in momentum space: Connection with Bloch oscillations, *Phys. Lett. A* **127**, 438 (1988).
- [50] X.-G. Zhao, R. Jahnke, and Q. Niu, Dynamic fractional Stark ladders in dc-ac fields, *Physics Letters A* **202**, 297 (1995); X.-G. Zhao, G. A. Georgakis, and Q. Niu, Rabi oscillations between Bloch bands, *Phys. Rev. B* **54**, 5235 (1996).
- [51] S. Longhi, M. Marangoni, M. Lobino, R. Ramponi, P. Laporta, E. Cianci, and V. Foglietti, Observation of dynamic localization in periodically curved waveguide arrays, *Phys. Rev. Lett.* **96**, 243901 (2006).
- [52] A. Eckardt, M. Holthaus, H. Lignier, A. Zenesini, D. Ciampini, O. Morsch, and E. Arimondo, Exploring dynamic localization with a Bose-Einstein condensate, *Phys. Rev. A* **79**, 013611 (2009).
- [53] R. B. Paris, An Inequality for the Bessel Function $J_\nu(\nu x)$, *SIAM J. Math. Anal.*, **15**, 203 (1984).
- [54] F. W. J. Olver, D. W. Lozier, and R. F. Boisvert, *NIST handbook of mathematical functions*, (Cambridge University Press, 2010).

Supplementary Material: Manipulating non-Hermitian skin effect via electric field

In the Supplementary Materials, we first give the details of deriving the analytical solutions of quantum dynamics. Then, we discuss the analytical results and obtain the effects of the pure dc field, pure ac field and the mixed field on the non-Hermitian skin effect. Finally, we discuss the finite size effect in the pure dc field case.

I. Analytical solutions of quantum dynamics

We derive the analytical solutions of quantum dynamics for our one-dimensional non-Hermitian model driven by an arbitrary time-dependent electric field $f(t)$. The Hamiltonian are following,

$$\hat{H}(t) = \sum_{m=-\infty}^{+\infty} (J_L|m\rangle\langle m+1| + J_R|m+1\rangle\langle m|) + f(t) \sum_{m=-\infty}^{+\infty} m|m\rangle\langle m|, \quad (\text{S1})$$

where J_R and J_L are the strengths of the left and right hopping, respectively. We expand the time-dependent quantum state as $|\psi(t)\rangle = \sum_{m=-\infty}^{+\infty} C_m(t)|m\rangle$ and substitute it into Schrödinger equation $i\partial_t|\psi(t)\rangle = \hat{H}(t)|\psi(t)\rangle$ (we set $\hbar = 1$ throughout this paper) to arrive at the equation of the time-dependent amplitudes $C_m(t) = \langle m|\psi(t)\rangle$,

$$i\partial_t C_m(t) = J_L C_{m+1}(t) + J_R C_{m-1}(t) + f(t) m C_m(t). \quad (\text{S2})$$

In solving Eq. (S2), we transfer to the momentum space first by the discrete Fourier transformation,

$$C_k(t) = \sum_{m=-\infty}^{+\infty} e^{-ikm} C_m(t), \quad (\text{S3})$$

and then we can directly rewrite Eq. (S2) as

$$\partial_t C_k(t) - f(t) \partial_k C_k(t) = -i (J_L e^{ik} + J_R e^{-ik}) C_k(t). \quad (\text{S4})$$

This partial differential equation can be transferred to an ordinary differential equation by the variables transformation

$$p = t, q = k + \eta(t), \quad (\text{S5})$$

with $\eta(t) = \int_0^t f(t') dt'$. This gives rise to $C_k(t) = C(p, \tau)$ with $\tau = q - \eta(p)$ and the chain rule of the derivation of $C(p, \tau)$ over p results in the ordinary differential equation,

$$\begin{aligned} \frac{dC(p, \tau)}{dp} &= \frac{\partial C(p, \tau)}{\partial p} \frac{\partial p}{\partial p} + \frac{\partial C(p, \tau)}{\partial \tau} \frac{\partial \tau}{\partial p}, \\ &= \frac{\partial C(p, \tau)}{\partial p} - f(p) \frac{\partial C(p, \tau)}{\partial \tau}, \\ &= -i (J_L e^{i\tau} + J_R e^{-i\tau}) C(p, \tau), \end{aligned} \quad (\text{S6})$$

where we applied Eq. (S4) to the last step. Eq. (S6) can be solved by integrating p over two sides and then

$$\begin{aligned} C(p, \tau) &= C(0, \tau|_{p=0}) e^{-i \int_0^p [J_L e^{i(q-\eta(p'))} + J_R e^{-i(q-\eta(p'))}] dp'}, \\ &= C(0, \tau|_{p=0}) e^{-i \int_0^p [(J_L + J_R) \cos(q-\eta(p')) + i(J_L - J_R) \sin(q-\eta(p'))] dp'}, \\ &= C(0, q) e^{-i \int_0^p [J_+ \cos(q-\eta(p')) + iJ_- \sin(q-\eta(p'))] dp'}, \end{aligned} \quad (\text{S7})$$

where $J_{\pm} = J_L \pm J_R$. Transferring Eq. (7) back to the form with variables (k, t) yields the solution of Eq. (S4),

$$C_k(t) = C_{k+\eta(t)}(0) e^{-i \int_0^t [J_+ \cos(k+\eta(t)-\eta(t')) + iJ_- \sin(k+\eta(t)-\eta(t'))] dt'}. \quad (\text{S8})$$

To simplify the solutions, we define the following functions

$$\mathcal{U}(t) = \int_0^t \cos[\eta(t) - \eta(t')] dt', \quad (\text{S9})$$

$$\mathcal{V}(t) = \int_0^t \sin[\eta(t) - \eta(t')] dt', \quad (\text{S10})$$

and the Eq. (S8) arrives at

$$\begin{aligned} C_k(t) &= C_{k+\eta(t)}(0) e^{-i[J_+(\mathcal{U} \cos k - \mathcal{V} \sin k) + iJ_-(\mathcal{U} \sin k + \mathcal{V} \cos k)] dt'}, \\ &= C_{k+\eta(t)}(0) e^{i(\bar{\mathcal{V}} \sin k - \bar{\mathcal{U}} \cos k)}. \end{aligned} \quad (\text{S11})$$

where

$$\bar{\mathcal{U}}(t) = J_+ \mathcal{U}(t) + iJ_- \mathcal{V}(t), \quad \bar{\mathcal{V}}(t) = J_+ \mathcal{V}(t) - iJ_- \mathcal{U}(t). \quad (\text{S12})$$

We apply the following expansions, which is expanded by ordinary Bessel functions $\mathcal{J}_m(x)$, to Eq. (S11) [1],

$$e^{-i\bar{\mathcal{U}} \cos k} = \sum_{m=-\infty}^{+\infty} e^{-i\frac{m\pi}{2}} e^{imk} \mathcal{J}_m(\bar{\mathcal{U}}), \quad (\text{S13})$$

$$e^{i\bar{\mathcal{V}} \sin k} = \sum_{m=-\infty}^{+\infty} e^{imk} \mathcal{J}_m(\bar{\mathcal{V}}), \quad (\text{S14})$$

and transfer the solutions in Eq. (S11) back to the spatial space by the discrete Fourier transformation,

$$C_m(t) = \sum_k e^{ikm} C_k(t). \quad (\text{S15})$$

Thus the time-dependent amplitude in spatial space $C_m(t)$ are

$$\begin{aligned} C_m(t) &= \sum_k e^{ikm} C_{k+\eta(t)}(0) e^{i(\bar{\mathcal{V}} \sin k - \bar{\mathcal{U}} \cos k)}, \\ &= \sum_k \sum_{n,r=-\infty}^{+\infty} e^{ik(m+n+r)} C_{k+\eta(t)}(0) e^{-i\frac{n\pi}{2}} J_n(\bar{\mathcal{U}}) J_r(\bar{\mathcal{V}}), \\ &= \sum_k \sum_{n,r=-\infty}^{+\infty} e^{i(k+\eta(t))r} C_{k+\eta(t)}(0) e^{-i\eta(t)r} e^{-i\frac{n\pi}{2}} J_n(\bar{\mathcal{U}}) J_{r-n-m}(\bar{\mathcal{V}}), \\ &= \sum_{n,r=-\infty}^{+\infty} C_r(0) e^{-i\eta(t)r} e^{-i\frac{n\pi}{2}} J_n(\bar{\mathcal{U}}) J_{r-n-m}(\bar{\mathcal{V}}), \\ &= \sum_{n,r=-\infty}^{+\infty} C_r(0) e^{-i\eta(t)r} e^{-i\frac{n\pi}{2}} J_n(\bar{\mathcal{U}}) e^{-i(n+m-r)\pi} J_{n+m-r}(\bar{\mathcal{V}}), \\ &= \sum_{r=-\infty}^{+\infty} (-1)^{m-r} C_r(0) e^{-i\eta(t)r} \left[\sum_{n=-\infty}^{+\infty} J_n(\bar{\mathcal{U}}) J_{n+m-r}(\bar{\mathcal{V}}) e^{i\frac{n\pi}{2}} \right], \\ &= \sum_{r=-\infty}^{+\infty} (-1)^{m-r} C_r(0) e^{-i\eta(t)r} \left(\frac{\bar{\mathcal{V}} + i\bar{\mathcal{U}}}{\bar{\mathcal{V}} - i\bar{\mathcal{U}}} \right)^{\frac{m-r}{2}} J_{m-r} \left(\sqrt{\bar{\mathcal{U}}^2 + \bar{\mathcal{V}}^2} \right). \end{aligned} \quad (\text{S16})$$

In the last step, we applied the Graf's addition theorem of the Bessel functions [1]. Through the relations in Eq. (S12), we can straightforwardly obtain that

$$\frac{\bar{\mathcal{V}} + i\bar{\mathcal{U}}}{\bar{\mathcal{V}} - i\bar{\mathcal{U}}} = \frac{J_R i\mathcal{V} - \mathcal{U}}{J_L i\mathcal{V} + \mathcal{U}}, \quad \bar{\mathcal{U}}^2 + \bar{\mathcal{V}}^2 = 2\sqrt{J_L J_R (\mathcal{U}^2 + \mathcal{V}^2)} = 2\sqrt{J_L J_R (u^2 + v^2)}. \quad (\text{S17})$$

Those expressions simplify the solution of Eq. (S16) to

$$C_m(t) = \sum_{r=-\infty}^{+\infty} (-1)^{m-r} C_r(0) e^{-i\eta(t)r} J_{m-r} \left(2\sqrt{J_L J_R [\mathcal{U}^2(t) + \mathcal{V}^2(t)]} \right) \left[\frac{J_R i\mathcal{V}(t) - \mathcal{U}(t)}{J_L i\mathcal{V}(t) + \mathcal{U}(t)} \right]^{\frac{m-r}{2}}. \quad (\text{S18})$$

This solution is valid for arbitrary initial state and for any time-dependent driven $f(t)$, and also can be specified to the system with finite long chains.

II. Discussions of the analytical results

Base on the exact analytical solution of quantum evolution in Eq. (S18), we can study the properties of the skin-effect and the electric fields induced Wannier Stark localization by choosing an appropriate initial state. Here, we set the system in site $m = 0$ as the specific initial state, i.e., $C_{m=0}(t = 0) = 1$, this is equivalent to set any other sites $m \neq 0$ as the initial state for the infinity long chain. Therefore, we can simplify the solution in Eq. (S18) and explicitly express the probability amplitude as,

$$\rho_m(t) = |C_m(t)|^2 = \mathcal{J}_m^2 \left(2\sqrt{J_L J_R [u^2(t) + v^2(t)]} \right) \left(\frac{J_R}{J_L} \right)^m, \quad (\text{S19})$$

where we used the relation $\mathcal{U}^2 + \mathcal{V}^2 = u^2 + v^2$ and here

$$u(t) = \int_0^t dt' \cos \eta(t'), \quad v(t) = \int_0^t dt' \sin \eta(t'). \quad (\text{S20})$$

We note that Eq. (S19) will become Eq.(5) of the main text when we choose the initial state localized at n_0 , i.e., $C_{m=n_0}(t = 0) = 1$ instead of $C_{m=0}(t = 0) = 1$. The exact solutions in Eq. (S19) are valid when $J_L J_R \neq 0$ and project to Hermitian case when $J_L = J_R$. In the Non-Hermitian cases $J_L \neq J_R$, the coefficients $(J_R/J_L)^m$ are responsible to the skin effect. Eq. (S19) is normalized for the Hermitian case, and for non-Hermitian cases, the addition normalization is needed.

Next, we consider the following electric fields

$$f(t) = E_0 + E_1 \cos \omega t, \quad (\text{S21})$$

where E_0 and E_1 are the strengths for the dc and ac parts, respectively. ω is the ac driven frequency. Under this driven, we have

$$\eta(t) = E_0 t + \frac{E_1}{\omega} \sin \omega t, \quad (\text{S22})$$

and then

$$u(t) = \int_0^t dt' \cos \left(E_0 t' + \frac{E_1}{\omega} \sin \omega t' \right), \quad v(t) = \int_0^t dt' \sin \left(E_0 t' + \frac{E_1}{\omega} \sin \omega t' \right). \quad (\text{S23})$$

$u(t)$ and $v(t)$ are not bounded functions only in the absence of electric fields, namely $f(t) = 0$. In this case, we have $u(t) = t$ and $v(t) = 0$, yielding $\rho_m(t) = \mathcal{J}_m^2 (2t\sqrt{J_L J_R}) (J_R/J_L)^m$, which gives purely skin effect due to the argument x in $\mathcal{J}_m(x)$ is linearly increasing to infinity and then $\mathcal{J}_m(x)$ approaches to vanish, such that only the probabilities of the edge sites survive by the coefficients $(J_R/J_L)^m$. This purely skin effect is shown in Fig. S1(b) through the quantum dynamic and as a comparison, the Hermitian case is shown in Fig. S1(a).

DC electric field

For this time-independent driven case $f(t) = E_0$, we have

$$u(t) = \frac{\sin E_0 t}{E_0}, \quad v(t) = \frac{1 - \cos E_0 t}{E_0}, \quad (\text{S24})$$

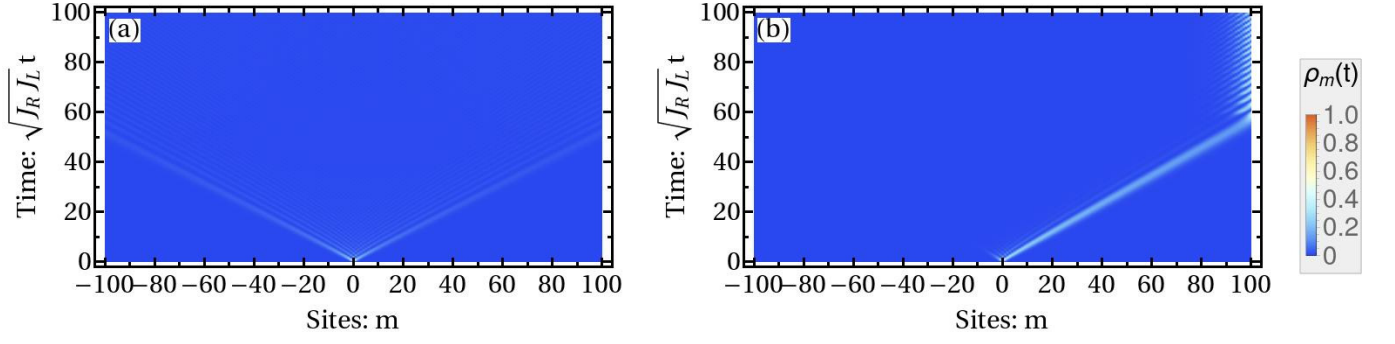


Figure S1: The quantum dynamics in the absence of fields for Hermitian case (a) : $J_L = J_R = 1.0$, and for the Non-Hermitian case (b) : $J_L = 0.8, J_R = 1.0$.

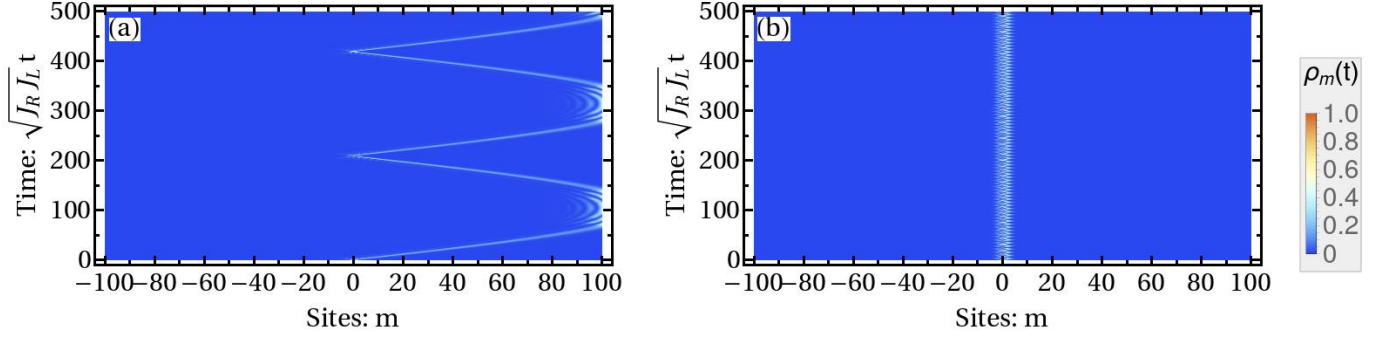


Figure S2: The quantum dynamics for the dc fields with the weakly driven (a) : $E_0 = 0.03$, and the strongly driven (b) : $E_0 = 1.0$. Other parameters are $J_L = 0.8, J_R = 1.0, \omega = 1.0$.

and the probability amplitude is

$$\rho_m(t) = \mathcal{J}_m^2 \left(\frac{4\sqrt{J_L J_R}}{E_0} \sin \frac{E_0 t}{2} \right) \left(\frac{J_R}{J_L} \right)^m. \quad (\text{S25})$$

From Eq. (S25), the argument of $\mathcal{J}_m(x)$ is bounded and oscillating along time when $E_0 \neq 0$. It means that the probability amplitude ρ_0 will oscillate back to 1 at the time points $t^* = 2\pi N/E_0$ with $N = 0, 1, 2, \dots$, due to the fact that $\mathcal{J}_m(0) = \delta_{m0}$. This Wannier Stark localization will compete with skin effect under the weakly driven shown in Fig. S2(a), and dominate the dynamics for the strongly driven shown in Fig. S2(b).

AC electric field

For this time-dependent driven case $f(t) = E_1 \cos \omega t$, we have

$$u(t) = \int_0^t dt' \cos \left(\frac{E_1}{\omega} \sin \omega t' \right), \quad v(t) = \int_0^t dt' \sin \left(\frac{E_1}{\omega} \sin \omega t' \right). \quad (\text{S26})$$

At each periodic cycles, i.e., $t^* = 2\pi N/\omega$ with $N = 0, 1, 2, \dots$, we have

$$u(t^*) = \frac{t^*}{\pi} \int_0^\pi d\tau \cos \left(\frac{E_1}{\omega} \sin \tau \right) = t^* \mathcal{J}_0 \left(\frac{E_1}{\omega} \right), \quad v(t) = 0, \quad (\text{S27})$$

and such that the probability amplitude at time t^* reads

$$\rho_m(t^*) = \mathcal{J}_m^2 \left(2t^* \sqrt{J_L J_R} \mathcal{J}_0 \left(\frac{E_1}{\omega} \right) \right) \left(\frac{J_R}{J_L} \right)^m, \quad (\text{S28})$$

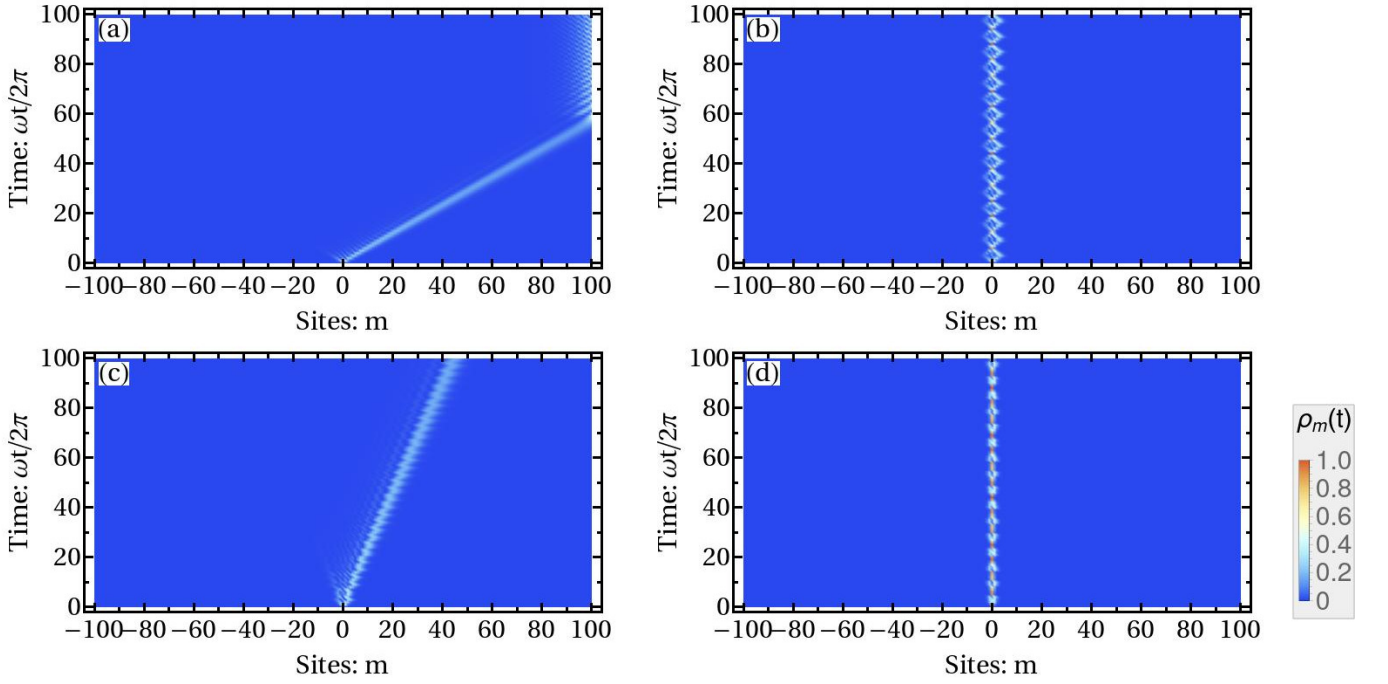


Figure S3: The quantum dynamics for the ac fields with the ratios (a) : $E_1/\omega = 0.1$, (b) : 0.2402 (1st zero of \mathcal{J}_0), (c) : 3.0, (d) : 5.52 (2nd zero of $\mathcal{J}_0(x)$). Other parameters are $J_L = 0.8$, $J_R = 1.0$, $\omega = 1.0$.

where shows that the system is localized only when E_1/ω is the zeros of J_0 , otherwise the skin effect will dominate the dynamics in the long time. To explicitly present this, we define two bounded functions as

$$\bar{u}(t) = u(t) - t\mathcal{J}_0\left(\frac{E_1}{\omega}\right), \quad \bar{v}(t) = v(t) - 0. \quad (\text{S29})$$

Then we rewrite the probability amplitude as

$$\rho_m(t) = \mathcal{J}_m^2 \left(2t \sqrt{J_L J_R \left[\mathcal{J}_0^2\left(\frac{E_1}{\omega}\right) + g_1(t)\mathcal{J}_0\left(\frac{E_1}{\omega}\right) + g_2(t) \right]} \right) \left(\frac{J_R}{J_L} \right)^m, \quad (\text{S30})$$

where $g_1(t) = 2\bar{u}(t)/t$ and $g_2(t) = (\bar{u}(t)^2 + \bar{v}(t)^2)/t^2$ are vanished at long time, and then we have

$$\rho_m(t \gg \frac{2\pi}{\omega}) \approx \mathcal{J}_m^2 \left(2t \sqrt{J_L J_R} \mathcal{J}_0\left(\frac{E_1}{\omega}\right) \right) \left(\frac{J_R}{J_L} \right)^m. \quad (\text{S31})$$

In Fig. S3, we take the ratio E_1/ω as two non-zeros of $\mathcal{J}_0(x)$ (a,c) where show the skin effect and as two zeros of $\mathcal{J}_0(x)$ in (b,d) where show the dynamical localization.

DC+AC electric field

The results above show that even weakly dc field will push the system to dynamical localization and while the ac field supports the skin effect except the ratio E_1/ω touches the zeros of Bessel function $\mathcal{J}_0(x)$. The competition between ac and dc fields in regard of localization will significantly modify the behaviors above.

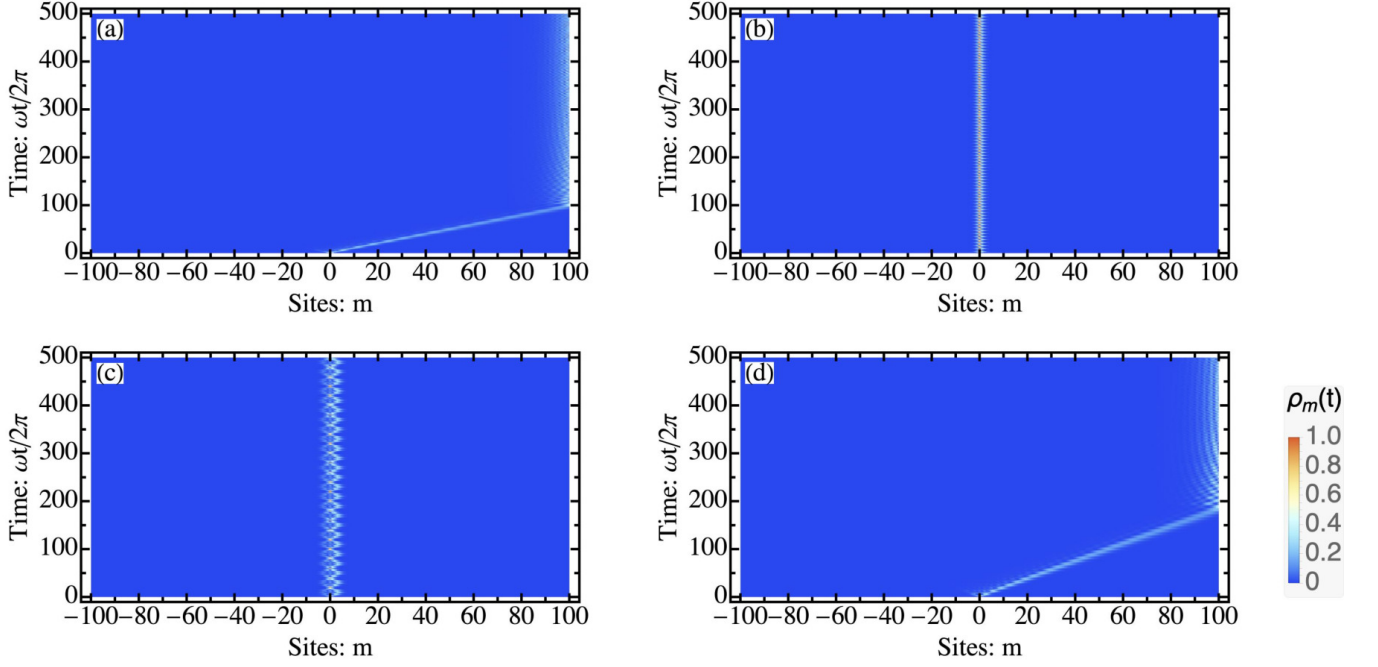


Figure S4: The quantum dynamics for the dc+ac fields with the ratios (a) : $E_0/\omega = 1.0$, $E_1/\omega = 2.0$, (b) : $E_0/\omega = 1.0$, $E_1/\omega = 3.832$ (1st zero of $\mathcal{J}_1(x)$), (c) : $E_0/\omega = 2.324$, $E_1/\omega = 2.0$, (d) : $E_0/\omega = 3.0$, $E_1/\omega = 3.0$. Other parameters are $J_L = 0.8$, $J_R = 1.0$, $\omega = 1.0$.

For this more general case, we first rewrite Eq. (S23) as ($\theta = \omega t$)

$$\begin{aligned} u(\theta) &= \frac{1}{\omega} \int_0^{\omega t} d\theta' \cos\left(\frac{E_0}{\omega}\theta' + \frac{E_1}{\omega}\sin\theta'\right), \\ &= \frac{1}{\omega} \int_0^{\omega t} d\theta' \left[\cos\left(\frac{E_0}{\omega}\theta'\right) \cos\left(\frac{E_1}{\omega}\sin\theta'\right) - \sin\left(\frac{E_0}{\omega}\theta'\right) \sin\left(\frac{E_1}{\omega}\sin\theta'\right) \right], \end{aligned} \quad (\text{S32})$$

$$\begin{aligned} v(\theta) &= \frac{1}{\omega} \int_0^{\omega t} d\theta' \sin\left(\frac{E_0}{\omega}\theta' + \frac{E_1}{\omega}\sin\theta'\right), \\ &= \frac{1}{\omega} \int_0^{\omega t} d\theta' \left[\sin\left(\frac{E_0}{\omega}\theta'\right) \cos\left(\frac{E_1}{\omega}\sin\theta'\right) + \cos\left(\frac{E_0}{\omega}\theta'\right) \sin\left(\frac{E_1}{\omega}\sin\theta'\right) \right], \end{aligned} \quad (\text{S33})$$

Applying the following relations [1],

$$\cos(z \sin \theta) = \mathcal{J}_0(z) + 2 \sum_{k=1}^{+\infty} \mathcal{J}_{2k}(z) \cos(2k\theta), \quad \sin(z \sin \theta) = 2 \sum_{k=0}^{+\infty} \mathcal{J}_{2k+1}(z) \sin[(2k+1)\theta], \quad (\text{S34})$$

and doing the integrating, we arrive at

$$u(t) = \frac{\sin(E_0 t)}{E_0} \mathcal{J}_0\left(\frac{E_1}{\omega}\right) + \sum_{k=1}^{+\infty} (-1)^k \mathcal{J}_k\left(\frac{E_1}{\omega}\right) \left[\frac{\sin(E_0 - k\omega)t}{E_0 - k\omega} + \frac{\sin(E_0 + k\omega)t}{E_0 + k\omega} \right], \quad (\text{S35})$$

$$\begin{aligned} v(t) &= \frac{1 - \cos(E_0 t)}{E_0} \mathcal{J}_0\left(\frac{E_1}{\omega}\right) + \frac{2}{\omega} \sum_{k=1}^{+\infty} \mathcal{J}_{2k}\left(\frac{E_1}{\omega}\right) \frac{\frac{E_0}{\omega} - \frac{E_0}{\omega} \cos(E_0 t) \cos(2k\omega t) - 2k \sin(E_0 t) \sin(2k\omega t)}{\left(\frac{E_0}{\omega}\right)^2 - 4k^2} \\ &\quad + \frac{2}{\omega} \sum_{k=0}^{+\infty} \mathcal{J}_{2k+1}\left(\frac{E_1}{\omega}\right) \frac{-(2k+1) + (2k+1) \cos(E_0 t) \cos[(2k+1)\omega t] + \frac{E_0}{\omega} \sin(E_0 t) \sin((2k+1)\omega t)}{\left(\frac{E_0}{\omega}\right)^2 - (2k+1)^2}. \end{aligned} \quad (\text{S36})$$

These expressions look very complicated and are difficult in doing the calculations continuously. Even so, we still can do some analysis depends on whether the ratio E_0/ω is an integer or not. If E_0/ω is not an integer, all the terms in

Eqs. (S35-S36) are bounded oscillatory functions of time such that the system will localize around the initial states. It means that the dc part of electric field dominate over the ac part and then indicate breaking of the skin effect. In the case of provided E_0/ω is an integer, function $v(t)$ in Eq. (S36) will not deduce any non-bounded functions and will have similar contributions as in the integer case. However, the functions $u(t)$ in Eq. (S35) takes (set $E_0 = \nu\omega$, $\nu \in Z$)

$$u(t) = (-1)^\nu \mathcal{J}_\nu \left(\frac{E_1}{\omega} \right) t + \frac{\sin(E_0 t)}{E_0} \mathcal{J}_0 \left(\frac{E_1}{\omega} \right) + \sum_{k=1, k \neq \nu}^{+\infty} (-1)^k \mathcal{J}_k \left(\frac{E_1}{\omega} \right) \left[\frac{\sin(E_0 - k\omega)t}{E_0 - k\omega} + \frac{\sin(E_0 + k\omega)t}{E_0 + k\omega} \right] \quad (\text{S37})$$

and then the first term is a non-bounded and linearly increasing function of time, such that at long time, we have

$$u(t \gg \frac{2\pi}{\omega}) \approx (-1)^\nu \mathcal{J}_\nu \left(\frac{E_1}{\omega} \right) t, \quad (\text{S38})$$

and the probability amplitude

$$\rho_m(t \gg \frac{2\pi}{\omega}) \approx \mathcal{J}_m^2 \left(2t\sqrt{J_L J_R} \mathcal{J}_{\frac{E_0}{\omega}} \left(\frac{E_1}{\omega} \right) \right) \left(\frac{J_R}{J_L} \right)^m, \quad (\text{S39})$$

which is merely replacing the order "0" in Eq. (S31) by E_0/ω .

As a conclusion, in this "dc+ac" case, the system will be featured in dynamical localization for all non-integer ratio E_0/ω (Fig. S4 (c)) and will be dominated by skin effect for all E_1/ω except zeros of $\mathcal{J}_{E_0/\omega}(x)$ when the ratio E_0/ω takes integer (Fig. S4 (a, b, d)). We show the parameters zone for the skin effect by the solid lines in Fig.3(a) in main text and all the rest zone are for dynamical localization.

III. Finite size effect for the pure dc case

In this section, we investigate the finite size effect in the pure dc field case. According to the inequality proven by Paris [2] for Bessel function, the probability $\rho_m(t)$ is bounded from above for big enough m ,

$$\rho_m(t) \leq \mathcal{J}_{m-n_0}^2(m-n_0) f_\chi^{m-n_0}(x_t). \quad (\text{S40})$$

Here $f_\chi(x_t) = x_t e^{1-\chi x_t}$, $\chi = \sqrt{J_L/J_R} < 1$, and $x_t = \frac{4J_R}{(m-n_0)|E_0|} |\sin \frac{E_0 t}{2}|$. The inequality holds if $4\sqrt{J_L J_R} \leq (m-n_0)|E_0|$. $f_\chi(x_t)$ is monotonically increasing and bounded $0 \leq f_\chi(x_t) \leq 1/\chi$, for $0 \leq x \leq 1/\chi$. There exists $0 \leq x_* < 1$ such that $f_\chi(x_*) = 1$ and $0 \leq f_\chi(x_t) < 1$ if $0 \leq x_t < x_*$. We also know $|\mathcal{J}_n(\bullet)| \leq 1$ [3]. Hence $\rho_m(t)$ would be insignificant if $4J_R \leq (m-n_0)|E_0|x_*$. Note that x_* depends only on J_L and J_R , and satisfies $x_* e^{1-\sqrt{J_L/J_R}x_*} = 1$. It is well known that $\mathcal{J}_{-n}(\bullet) = (-1)^n \mathcal{J}_n(\bullet)$. Adding the fact that $J_R > J_L$, $\rho_m(t)$ would be even less significant, if $m < n_0$ and $4J_R \leq |(m-n_0)E_0|x_*$. Therefore, in an infinite lattice, an electron would oscillate around its initial position n_0 within a range of $4J_R/|E_0|x_*$.

* These authors contribute equally to this work.

† Corresponding author: wangyc3@sustech.edu.cn

[1] G. N. Watson, A Treatise on the Theory of Bessel Functions, Cambridge Mathematical Library (Cambridge University Press, 1995).

[2] R. B. Paris, An Inequality for the Bessel Function $J_\nu(\nu x)$, SIAM J. Math. Anal., **15**, 203 (1984).

[3] F. W. J. Olver, D. W. Lozier, and R. F. Boisvert, NIST handbook of mathematical functions, (Cambridge University Press, 2010).